Edinburgh Research Explorer

Somatic activating mutations in Pik3ca cause sporadic venous malformations in mice and humans

Title: Somatic Mutation in *Pik3ca* Causes Sporadic Venous Malformations

Authors: Sandra D. Castillo[1],*, Elena Tzouanacou[2,3], May Zaw-Thin[4], Inma M. Berenjeno[1], Victoria E.R. Parker[5], Iñigo Chivite[6], Maria Milà-Guasch[1], Wayne Pearce[1], Isabelle Solomon[1], Robert E. Dewhurst[2], Rachel G. Knox[5], Cheryl L. Scudamore[7], Adam Badar[4], Tammy L. Kalber[4], Julie Foster[8], Daniel J. Stuckey[4], Anna David[9], Wayne A. Phillips[10], Mark F. Lythgoe[4], Valerie Wilson[2], Robert K. Semple[5], Neil J. Sebire[11], Veronica A. Kinsler[11], Mariona Graupera[6],† & Bart Vanhaesebroeck[1],*, †

Affiliations:
[1]UCL Cancer Institute, University College London, London, UK
[2]MRC Centre for Regenerative Medicine, School of Biological Sciences, The University of Edinburgh, Edinburgh, UK
[3]Institut Pasteur, Département de Biologie du Developpement, CNRS URA 2578, Paris, France
[4]Centre for Advanced Biomedical Imaging, University College London, London,UK
[5]Institute of Metabolic Science, University of Cambridge, Addenbrooke's Hospital, Cambridge, UK
[6]Vascular Signalling Laboratory, Institut d´Investigació Biomèdica de Bellvitge (IDIBELL), Barcelona, Spain
[7]Mary Lyon Centre, MRC Harwell, Harwell, UK. [8]Barts Cancer Institute, Queen Mary University of London, London, UK
[9]UCL Institute for Women's Health, London, UK
[10]Surgical Oncology Research Laboratory, Peter MacCallum Cancer Centre, Melbourne, Australia
[11]Great Ormond Street Hospital for Children, NHS Foundation Trust, London, UK.

* To whom correspondence should be addressed: S.D.C. (sandra.castillo@ucl.ac.uk) or B.V. (bart.vanh@ucl.ac.uk)

†Joint Last Authors

One Sentence Summary: Mutant *Pik3ca* gives rise to venous malformations in mouse and human

Abstract

Venous malformations (VMs) are painful and deforming vascular lesions composed of dilated veins, present from birth. Mutations in the tyrosine kinase receptor TIE2 have been found in approximately half of sporadic (non-familial) VMs, with the cause of the other cases unknown. Sclerotherapy, widely accepted as first-line treatment, is not fully efficient and targeted therapy for this disease remains underexplored. By mosaic expression in the embryonic mesoderm of *Pik3ca*[H1047R], a constitutively active mutant of the p110α isoform of PI 3-kinase (PI3K), we have

generated a genetically-engineered mouse model with vascular lesions present in newborn pups, which faithfully mirrors human VMs. In line with this, we (and Castel *et al.*, in the accompanying paper) have found activating *PIK3CA* mutations in human VMs, mutually exclusive with TIE2 mutations. Endothelial cell (EC)-specific expression of *Pik3ca*[H1047R] in newborn mice resulted in EC hyperproliferation and impaired pericyte coverage, both of which could be normalized by PI3K pathway inhibition by rapamycin. Moreover, *in vivo* rapamycin therapy led to regression of mesodermally-induced *Pik3ca*[H1047R] VMs. Our data demonstrate a causal relationship between activating *Pik3ca* mutation and the genesis of VMs, provide the first genetic model that faithfully mirrors the normal etiology and development of this human disease and establish proof-of-principle for the use of PI3K-targeted therapies in VMs.

Introduction

The PI3K family of enzymes signal downstream of a variety of cell surface receptors to regulate multiple cellular functions, including growth and proliferation *(1)*. *PIK3CA* (OMIM171834), the gene that encodes the p110α isoform of phosphoinositide 3-kinase (PI3K), is frequently mutated in epithelial cancer *(2)*. *PIK3CA* has recently been shown to undergo a similar range of activating mutations in non-cancerous disease conditions, such as in a spectrum of regional overgrowth disorders *(3-6)* (which have now been designated under the umbrella term *PIK3CA*-Related Overgrowth Spectrum (PROS) disease *(7)*) and in isolated (i.e. not-associated with overgrowth) lymphatic malformations (LMs) *(8)*. The *PIK3CA* mutations present in PROS and LMs are similar to those in solid tumors, with the H1047R mutation in the catalytic domain being the most prevalent *(8,9)*. In contrast to cancer, in which *PIK3CA* mutations are almost exclusively present in epithelial tissues, *PIK3CA*-mutant tissues in LMs and PROS are largely of mesodermal origin and mutations often present in a mosaic pattern. In this study, we report the presence of somatic *PIK3CA* mutations in another human disease condition of mesodermal origin, namely isolated

VMs. We also created a genetically-modified mouse model that displays mutant *Pik3ca*-driven congenital vascular malformations with features pathognomonic for human VMs, but has no other type of overgrowth or malformations.

VMs are the most common vascular malformations, with an overall incidence of 1/5000 *(10)*. VMs are usually congenital lesions that consist of dilated venous channels with scarce mural cell coverage. These VMs can be of different sizes and affect any tissue, such as subcutaneous tissue or internal organs. VMs are painful and disfiguring, many lead to bleeding and obstruction of organs, and in some cases to localized intravascular coagulopathy and pulmonary embolism *(11,12)*. Treatment of VMs mainly consists of alleviation of symptoms using compression garments when possible, but curative treatment remains seldom possible. At present, sclerotherapy is the mainstay therapy to diminish the volume of VMs, but it causes several side effects and is not fully efficient *(12)*.

Mutations in the *TEK* gene, coding for the endothelial tyrosine kinase receptor TIE2, are known to cause about half of sporadic VMs *(13)*, the other half remaining unknown. Here, in a small cohort of patients diagnosed with sporadic VMs, without any associated overgrowth or other vascular malformation component, we found a *PIK3CA*-activating mutation in a VM that is wild-type for the *TEK* gene. This was corroborated by a larger study in the accompanying paper by Castel *et al.* in which *PIK3CA* mutations were found in 25% of the VMs analysed, in a mutually exclusive manner to previously identified mutations in *TEK (14)*. The finding that mutation in *PIK3CA* plays a key role in the pathogenesis of VMs provides guidance for refined diagnosis for this disease and a possible targeted therapeutic avenue using PI3K pathway inhibitors.

Results

Mosaic *Pik3ca^{H1047R}* expression in embryonic mesoderm leads to VMs in mice

In this study, we set out to investigate the effects of *Pik3ca* mutation in mesodermal tissue in mice. Given that all known disease conditions of mesodermal origin currently associated with *PIK3CA* mutation are congenital or early childhood onset, we induced expression of mutant *Pik3ca* in the embryonic mesoderm. To further adequately model the human disease context, mutant *Pik3ca* expression was induced in a mosaic fashion, in the heterozygous state and from its endogenous promoter *(15)*. We reasoned that such tissue-restricted mosaic induction could also avoid the detrimental effect of ubiquitous expression of mutant *Pik3ca* during embryonic mouse development *(16)*. The mutant used for these experiments is *Pik3ca^{H1047R}* which encodes the H1047R hot-spot mutation found in cancer *(2)*, LMs *(8)* and PROS *(9)*.

For these studies, we generated the *T-CreER^{T2}* mouse line by introducing a transgene (**Supplementary Fig. 1A**) that drives the expression of a 4-hydroxytamoxifen (4-OHT)-inducible Cre recombinase under the control of the previously characterized promoter of the *T* gene *(17)*. The *T* gene encodes the Brachyury transcription factor that is transiently expressed in the nascent embryonic mesoderm *(18)*. To evaluate Cre activity, we crossed *T-CreER^{T2}* mice with *Rosa26-lacZ* reporter mice *(19)* that ubiquitously express the floxed *lacZ* gene expression cassette from the *Rosa26* locus (**Supplementary Fig. 1B**), and stained for lacZ expression following treatment of mice with 4-OHT. We administered 4-OHT to pregnant females between embryonic day (E) 7.5 and 10.5. Induction of Cre at E7.5 led to a widespread activity of Cre recombinase in the mesoderm, in a 4-OHT dose-dependent manner, which was mosaic except at the higher doses tested (**Supplementary Fig. 1C, D**).

We next crossed *T-CreER^{T2}* mice to mice that are heterozygous for a Cre-inducible knock-in allele of *Pik3ca^{H1047R}* (Ref. *(15)*), followed by mosaic *Pik3ca^{H1047R}* induction at E7.5 using different doses of 4-OHT (**Fig. 1A**). Interestingly, several of these mice [hereafter referred to as MosMes-

Pik3ca^{H1047R} (Mosaic Mesodermal-*Pik3ca^{H1047R}*) mice] were born with subcutaneous vascular malformations in different body sites, with no apparent overgrowth in other tissues (**Fig. 1B**), nor alterations in body weight, organ size or tissue histology (tested up to 6 months of age), compared to wild-type (WT) littermates that had also been treated with 4-OHT (**Supplementary Fig. 2; Supplementary Table S1**). This phenotype was not fully penetrant at lower 4-OHT doses, but increased in a dose-dependent manner (**Supplementary Table S2**). The lower doses of 4-OHT tested gave rise to localized vascular lesions, whereas the higher doses, possibly due to the higher probability of targeting multiple EC progenitors, induced multifocal, diffuse and more severe malformations (**Fig. 1B**). High 4-OHT doses also led to a lower than expected Mendelian distribution of mutant mice (**Supplementary Table S3**), with some of the mutant embryos displaying vascular developmental defects (**Supplementary Fig. 3**). Our observation on the lethality and vascular defects in *Pik3ca^{H1047R}* embryos are similar to the previously reported phenotypes of ubiquitous or EC-specific expression of *Pik3ca^{H1047R}* in the developing embryo *(16)*.

Computed Tomography Angiography (CT-A) analysis of adult MosMes-*Pik3ca^{H1047R}* mice confirmed the presence of subcutaneous vascular malformations and revealed additional internal vascular malformations in the mesentery (not shown) and urogenital area (**Fig. 1C**), similar to those observed in some patients. Some of these mice also displayed rectal bleeding, as observed also in the human condition. Mice with the most prominent vascular malformations also displayed phlebectasias of the portal vein and inferior *vena cava* (**Fig. 1C**), similar to those observed in patients with predominantly venous vascular malformations (reviewed in Ref. *(20)*). Additional scanning of blood flow in the vascular malformation by power Doppler ultrasound indicated that the contribution of flow was primarily venous in origin (slow flow) (**Supplementary Fig. 4**). This was corroborated by histological analysis which showed that the vascular lesions in MosMes-*Pik3ca^{H1047R}* mice were poorly circumscribed, non-encapsulated lesions composed of blood-filled, predominantly thin-walled, irregular and variably sized vascular channels interposed between

normal tissues (**Fig. 1D**). Some channels contained organising fibrin thrombi, with focal interstitial haemorrhage present. Altogether, these observations point to a diagnosis of VMs in MosMes-*Pik3ca*^{H1047R} mice, with a pathology and disease burden similar to those observed in humans with VMs.

PIK3CA is mutated in human VMs

Our findings in mice of a causative role of *Pik3ca* mutation in VM led us to explore the presence of *PIK3CA* mutations in human VMs. As a proof of principle, we analysed *PIK3CA* and *TEK* genes by deep sequencing (mean coverage of 2000x) in a small cohort of human sporadic VMs that had no associated overgrowth or other vascular malformation component. Among the VMs sequenced, one had a mutation in *PIK3CA* and other two were mutant for *TEK*, with an allelic frequency of 5-10% (**Table 1**). Interestingly, mutations in *PIK3CA* and *TEK* were mutually exclusive. The observed *TEK* mutations have already been described for VMs *(21)*. The mutation found in *PIK3CA* (E545K), is a hot-spot mutation in cancer *(2)*, PROS *(9)* and LMs *(8)*. In line with our observations, Castel *et al.*, (in the accompanying manuscript *(14)*) found, in a larger cohort of VMs, that *PIK3CA* was mutated in 25% of the samples. These *PIK3CA* mutations, of which the H1047R and E542K hot-spot mutations were the most frequent, were mutually exclusive with *TEK* mutations, present in 35% of the VMs analysed. These findings suggest that *PIK3CA* might be a relevant diagnostic marker for human VMs.

Endothelial activation of _Pik3ca_ promotes hyperproliferation in ECs and inhibits pericyte coverage

ECs, being the main cell type in blood vessels, are thought to be important in VM development. Given the important role for *Pik3ca* in EC biology *(22-25)*, we decided to selectively test the impact of *Pik3ca*^{H1047R} expression in ECs. To this end, we generated EC-*Pik3ca*^{H1047R} mice by

crossing conditional heterozygous *Pik3ca*$^{WT/H1047R}$ mice onto *Pdgfb-iCreER* mice that express 4-OHT-inducible Cre specifically in ECs (Ref. *(26)*) (**Supplementary Fig. 5**). 4-OHT was administered to EC-*Pik3ca*^{H1047R} pups on postnatal day 1 (P1), and retinal angiogenesis was analyzed five days later (**Fig. 2A**). Staining of P6 retinas with isolectin-B$_4$ (IB4; which binds to the EC plasma membrane) revealed that endothelial expression of *Pik3ca*^{H1047R} resulted in dramatic hyperplasia, with individual vessels no longer being discernible, correlating with increased numbers and proliferation of ECs (**Fig. 2B, C**). Radial expansion of the vascular bed was also decreased upon endothelial expression of *Pik3ca*^{H1047R}, possibly due to EC hyperplasia, (**Fig. 2D, E**) whereas sprouting angiogenesis was not affected (**Fig. 2F**). In addition, EC-*Pik3ca*^{H1047R} lungs showed reduced mRNA expression of *Ephb4*, *Efnb2* and *Nr2f2*, key genes involved in arteriovenous specification *(27)*, suggesting that oncogenic *Pik3ca* compromises arteriovenous identity (**Fig. 2D**).

A distinctive feature of VMs is the poor presence, or even absence, of mural cells *(28)*. Proper homeostasis of vessels requires a tight interplay between ECs and their supporting mural cells, which are perivascular cells represented by two cell types, vascular smooth muscle cells (vSMCs) and pericytes. Both cell types are differently distributed over the vasculature, with vSMCs typically present in large vessels whereas pericytes are mainly localized in the microvasculature *(29)*. In EC-*Pik3ca*^{H1047R} retinas, pericytes (NG2-positive cells) were conspicuously absent from the vascular front and very sparse in the plexus where they were poorly associated with the vessels, in contrast with *Pik3ca*^{WT} retinas that showed a typical attachment of pericytes to the EC surface with multiple extensions (**Fig. 2G**). Defective mural cell coverage was also observed in the VMs from MosMes-*Pik3ca*^{H1047R} mice (**Fig. 1D**). Pdgfb, which is produced by ECs, is the major attractant for mural cells *(30)* and is expressed at lower levels in human TIE2-mutant VMs *(31)*. The Foxo1 transcription factor, which is negatively regulated by PI3K activity, stimulates Pdgfb expression. In line with this, analysis of total mRNA isolated from lungs, a tissue highly enriched in ECs, showed a decrease in Pdgfb expression in EC-*Pik3ca*^{H1047R} compared to *Pik3ca*^{WT} mice (**Fig. 2H**). The

pericyte phenotype observed in EC-*Pik3ca^{H1047R}* retinas is reminiscent of that observed in the so-called Pdgfb-retention motif knock-out mice, in which pdgfb produced by the ECs is not retained at the surface *(32)*.

Taken together, *Pik3ca^{H1047R}* expression in ECs results in ECs hyperproliferation and vessel hyperplasia, loss of arteriovenous identity and defective pericyte coverage.

Rapamycin reduces *Pik3ca^{H1047R}*-EC hyperproliferation, rescues pericyte coverage and induces regression of *Pik3ca^{H1047R}*-driven VMs *in vivo*

At the moment, there are no targeted therapies for VMs. Rapamycin and its analogs are approved drugs for compassionate use in human therapy of vascular anomalies *(33-39)*. Rapamycin interferes with signalling downstream of PI3K by inhibition of mTOR *(40)*. To test the effect of rapamycin in *Pik3ca^{H1047R}* ECs *in vivo*, we treated EC-*Pik3ca^{H1047R}* pups with rapamycin (administered together with 4-OHT and 8 h prior to analysis of retinal angiogenesis; **Fig. 3A**). Rapamycin prevented retinal vascular hyperplasia, reducing the number of ECs and proliferation (**Fig. 3B, C**), and normalised pericyte coverage in both the vascular front and plexus of EC-*Pik3ca^{H1047R}* retinas (**Fig. 3D**). Rapamycin also diminished vessel area and number of ECs in *Pik3ca^{WT}* retinas, in line with its previously documented anti-angiogenic effects *(41)*, without affecting EC proliferation (**Fig. 3B, C**).

To take these observations closer to the disease context, we treated an adult MosMes-*Pik3ca^{H1047R}* mouse with a large VM with rapamycin (**Fig. 4A**). The dose chosen for this study (4 mg/kg every other day) was based on previous studies using long-term rapamycin treatment *(42,43)*. Rapamycin treatment reduced the volume of the vascular lesion after two weeks of treatment, as assessed by CT-A (**Fig. 4B**). By the fourth week of treatment, the VM had largely regressed (**Fig. 4B**) and was no longer detectable upon necropsy that was performed immediately following the last imaging. A partial reduction of the phlebectasia in the portal vein and inferior

vena cava were also seen after rapamycin treatment (**Fig. 4C; Supplementary Fig. 6**). These data suggest that PI3K pathway intervention might be an effective therapeutic option for human *PIK3CA*-driven VMs.

Discussion

Here we report on a genetic mouse model for human VMs and demonstrate that somatic, mosaic expression of an activating mutation (H1047R) in *Pik3ca* in the embryonic mesoderm of mice can induce and maintain VMs. Previous mouse models of VM used transgenic expression of a murine viral oncogene *(44)* or xenotransplantation into nude mice of either human vascular endothelial cells (HUVECs) transduced with mutant TIE2 *(39)* or the MS1 immortalized endothelial cell line expressing mutant Akt1 *(45)*. Xenograft models do not take into account the developmental origin and natural progression of the human disease. Yet, our mosaic mesodermal VM mouse model shows some limitations for use in standardized uniform cohort therapeutic experiments, namely some degree of embryo lethality, a variable penetrance of the VM phenotype and a wide heterogeneity of VMs in terms of size, localization and expansion. However, these limitations of our mouse model adequately reflect the characteristics of this human disease, with every patient showing a distinct disease pattern and progression, most likely due to the spatially and temporally distinct and mosaic acquisition of the mutation leading to the disease. Of note, activation of PI3K signalling in adult mice, either by ubiquitous expression of mutant *Pik3ca (46)* or EC-specific expression of transgenic activated *Akt1* leads to increased blood vessel size and permeability, without inducing VMs *(41)*. This underscores the concept that VMs arise as a result of genetic errors during embryonic development.

Mechanistically, our data suggest that VMs are likely to develop as a result of *Pik3ca^{H1047R}*-induced enhancement of EC proliferation. VMs might develop as errors in endothelial precursors during embryonic vasculogenesis. Indeed, EC hyperproliferation during vasculogenesis has

previously been shown to give rise to vessel hyperfusion, and to result in dilated, dysfunctional vessels, similar to those found in VMs *(47,48)*. Another typical feature of VMs is poor mural cell coverage *(28)*. Here, we also show that *Pik3ca^{H1047R}* expression in ECs inhibits pericyte attachment likely due to the decreased expression of Pdgfb, which is necessary for pericyte coverage *(49)*. This might therefore also contribute to the genesis of VMs upon *Pik3ca* mutation. On top of reducing mural cell coverage, *Pik3ca^{H1047R}* might also contribute to the formation of VMs by preventing arteriovenous identity as seen by decreased expression of arteriovenous differentiation markers *(50)*.

At present, it is not clear why widespread mosaic induction of *Pik3ca^{H1047R}* in the mouse mesoderm gives rise to malformations solely in the vasculature and does not induce obvious overgrowth or malformation in other tissue compartments. This might be due to the chosen strategy (timing and tissue location) of *Pik3ca^{H1047R}* gene induction. However, Castel *et al*. (in the accompanying manuscript) have made similar observations in their models *(3)*. One explanation could be the previously reported exceptional sensitivity of ECs to PI3K pathway deregulation *(22-25)*. Also intriguing is the dominant venous character of the vascular malformations observed in *Pik3ca^{H1047R}* mice. This could arise as a consequence of the known role of PI3K activation in driving venous over arterial signalling during vasculogenesis *(51)*.

In addition, the human genetic data presented here and in the accompanying manuscript *(14)* reveal the presence of *PIK3CA* mutations in VMs, mutually exclusive with mutations in the TIE2 tyrosine kinase receptor that were discovered over 20 years ago *(28)*. Our studies thus uncover and document the potential for a new targeted therapy in human VMs, and the potential for repurposing of p110α inhibitors currently being developed for cancer treatment. An important consideration is how diagnosis of *TEK*/TIE2 and *PIK3CA* mutations in VMs can influence the treatment of this disease using targeted agents. The wild-type TIE2 receptor tyrosine kinase is known to signal through both PI3K and MAPK signalling pathways in ECs *(52,53)*. TIE2-mutant cells show chronic

activation of the MAPK pathway and respond very well to its inhibition *(54)* but, surprisingly, not to TIE2 kinase inhibitors *(39)*. Our studies identify a subpopulation of patients with *PIK3CA* mutant VMs, which will most likely be non-responsive to TIE2 or MAPK kinase inhibitors. However, like the TIE2-mutant VMs *(39)*, *PIK3CA*-mutant VMs are expected to respond to PI3K inhibitors or rapamycin. It is also likely that TIE2 mutant VMs will benefit from treatment with PI3K inhibitors in combination with MAPK inhibitors.

In conclusion, our findings in mice have led us to discover the presence of *PIK3CA* mutations in a new human disease. VMs join the growing list of diseases where the presence of activating *PIK3CA* mutations, commonly associated with cancer, leads to tissue malformation, without leading to malignancy *(8,9)*. Our finding that mutation in *PIK3CA* plays a key role in the pathogenesis and maintenance of VMs provides guidance for improved diagnosis for this disease and a possible new targeted therapeutic avenue using PI3K pathway inhibitors.

Materials and Methods

Study design

This study was designed to test the effect of *Pik3ca^{H1047R}* expression in the embryonic mesoderm of mice. We obtained sufficient data on mice to determine that this leads to VMs. To translate these findings to the human context, we tested *PIK3CA* mutation in human VMs and found that this gene is mutated in this disease. For this, well-characterized patients with confirmed VMs and without any associated overgrowth or malformation were recruited at Great Ormond Street Hospital, London, UK. All patients provided informed consent. In addition, to better understand the mechanisms underlying the role of *Pik3ca^{H1047R}* in ECs, we performed mouse retinal angiogenesis studies as a vascular biology read-out. For these experiments, power analysis on preliminary data was performed, suggesting a minimal cohort size of n=4-6 to observe a medium difference with 80% power, depending on the type of experiment. The sample size for each experiment is indicated in the corresponding figure legend. Given that n was <10, non-parametric tests were applied. All mechanistic studies were performed without randomization or blinding. Exclusion criteria were only applied to data shown in Fig. 4 (rapamycin treatment of mouse harbouring VMs): only mice that were deemed to be sufficiently fit to tolerate the treatment were included in the experiment. This is in line with UK Home Office regulations.

Subjects

This study was approved by the UK National Research Ethics Committee. Written informed consent was obtained from all participants or their parents. Tissues from individuals diagnosed as having sporadic VMs, not associated with other syndromes, were investigated. Genomic DNA was extracted from lesions using standard procedures.

Next generation sequencing with preceding target enrichment

Sequencing of *TEK* and *PIK3CA* was performed using Next Generation Sequencing with preceding target enrichment. All equipment and materials were purchased from Life Technologies, Thermo-Fisher Scientific. In brief, DNA was quantified using Qubit® and libraries were prepared using the Ion AmpliSeq Library 96 Kit 2.0 with 10 ng of genomic DNA in each reaction. This involved an initial PCR reaction to amplify genomic targets using a custom-designed primer pool which provides coverage of all coding regions of *PIK3CA* and *TEK*. Samples were then partially digested prior to ligation of barcode adaptors and emulsion PCR. Enrichment steps were carried out using the Ion OneTouch 200 Template Kit v2 and the amplicon libraries were sequenced on an Ion Torrent Personal Genome Machine system using 318 chips, and bar-coding was applied with an Ion Xpress Barcode Adapters 1–16 Kit. Ion Reporter® software was used to analyse data, or alternatively Bam files were uploaded and viewed in the Integrative Genomics Viewer, Broad Institute (http://www.broadinstitute.org/igv/). The mean depth of coverage for sequencing was 2000X.

Reagents

Primary antibodies to the following proteins were used: Erg (ab92513; Abcam), NG2 (AB5320; Merck Millipore), endomucin (sc-65495; Santa Cruz Biotechnology). Secondary antibodies conjugated to Cy3, Cy5 or AlexaFluor 647 were from Jackson ImmunoResearch Laboratories. Isolectin GS-IB$_4$ conjugated to AlexaFluor 488 (I21411) or AlexaFluor 568 (I21412) (further referred to as IB4) were from Life Technologies. Immu-Mount mounting media was from Thermo Scientific. AuroVist 15 nm gold nanoparticles were from Nanoprobes Inc. Rapamycin used for therapeutic studies was obtained from Merck Millipore. All chemicals, unless otherwise stated, were from Sigma-Aldrich.

Mice

Mice were housed in individually-ventilated cages and cared according to UK Home Office guidelines and legislation, with procedures accepted by the Ethics Committees of University College London and Queen Mary University of London. All mice used were backcrossed on a C57BL/6 background for more than 12 generations. *Pik3ca*$^{WT/H1047R}$ mice harbour a germline *Pik3ca* allele with a conditional H1047R mutation *(15)*. In these mice, Lox*P* sites flank exon 20 of *Pik3ca*, which, upon Cre recombination, is replaced by a downstream copy of exon 20 containing a CAT to AGG change in codon 1047. *Pdgfb-iCreER* mice *(26)* express an inducible iCreER recombinase from the endogenous *Pdgfb* locus.

Generation of the *T-CreER*^{T2} mouse line

The pTcreER^{T2} vector **Supplementary Fig. S1** comprising the *T* regulatory sequence from -1050 bp to +140 bp (Ref.*(17)*) was inserted upstream of a *CreER*^{T2} sequence. To eliminate uninduced background activity of Cre in the absence of 4-OHT, the *nls* sequence at the 5' of *CreER*^{T2} was removed. This plasmid was *FspI*-linearized and electroporated into E14TG2a ES cells as described previously *(55)*. After 10 days of selection with Hygromycin (140 μg/ml), resistant clones were isolated, expanded and screened by Southern blot to verify integration of the transgene and to identify ES clones with single and multiple insertions of the transgene. Clones were tested in parallel by *in situ* hybridisation for Cre expression in differentiating ES cells. Four clones (three with a single integration and one with two integrations) that showed the characteristic spatial pattern of *T* expression in differentiating ES cell monolayers (as explained in Ref.*(56)*) were selected for further analysis. Absence of uninduced background recombination and 4-OHT-induced Cre recombination in these four clones were tested *in vitro* by transient transfection of a Cre-conditional Egfp transgene (pPHCAG-C2-egfp, a gift from Austin G. Smith, Wellcome Trust - Medical Research Council Cambridge Stem Cell Institute, UK). Clones with single *T-CreER*^{T2}

integration showed efficient recombination upon treatment with 0.2 μM or 1 μM of 4-OHT, with virtually no background of uninduced recombination. These clones were injected into C57BL/6 host blastocysts and chimeric male offspring mated to C57BL/6 females. F1 heterozygotes were identified by coat colour and PCR amplification of the Cre sequence. Offspring were backcrossed for >5 generations to C57BL/6 mice before generating a homozygote *T-CreER^T2* line by intercrossing. Following further characterization by crosses with *Rosa26-lacZ* reporter mice*(19)*, one *T-CreER^T2* mouse line (number 53) was maintained and established in the homozygote state.

Mesoderm- and EC-specific *Pik3ca^H1047R* expression in mice

Mesoderm-specific mosaic expression of *Pik3ca^H1047R* (MosMes-*Pik3ca^H1047R* mice) was achieved by crossing *Pik3ca^WT/H1047R* mice with *T-CreER^T2* mice. To induce mosaic Cre activation, pregnant females were given varying doses of 4-OHT (12.5 to 250 μg, from a stock solution of 10 mg/ml, diluted in 1:1 absolute ethanol-Kolliphor®EL) with 200 μl of PBS added for intraperitoneal injection at E7.5 (E0.5 relates to the female presence of a vaginal plug indicating that the mating occurred the night before). Progesterone (dissolved in Kolliphor®EL) was co-administered at half the total dose of 4-OHT given, in order to avoid undesirable oestrogen agonist effects of 4-OHT, which can result in late fetal abortions in pregnant mice. Postnatal EC-specific expression of *Pik3ca^H1047R* was achieved by crossing *Pik3ca^WT/H1047R* with *Pdgfb-iCreER* mice. To induce Cre activation, newborn pups (P1) were injected intragastrically with 5 μg 4-OHT (dissolved in absolute ethanol).

Whole-mount embryo X-gal staining

Freshly isolated E12.5 embryos were fixed in 4% paraformaldehyde on ice for 30 min, washed (3 x 10 min) in PBT (PBS with 0.1% Tween) and stained for 48 h at 30ºC in X-gal staining solution (4 mM potassium ferricyanide, 4 mM potassium ferrocyanide, and 2 mM $MgCl_2$, 1 mg/ml X-gal in

PBT). After staining, embryos were washed (3 x 10 min) in PBS, post-fixed in 4% paraformaldehyde for $\geq$ 1 h and mounted.

Whole-mount embryo immunofluorescence

Freshly isolated E9.5 embryos were fixed in 4% paraformaldehyde overnight at 4°C. After washing in PBT, embryos were dehydrated in increasing concentrations of methanol (50%, 80% methanol/PBT, 100% methanol), rehydrated in decreasing concentrations of methanol, followed by a 30 min wash in Pblec buffer (0.2 mM $CaCl_2$, 0.2 mM $MgCl_2$, 0.2 mM $MnCl_2$ and 2% Triton X-100 in PBS) and overnight incubation at 4°C with antibody to endomucin, diluted 1:20 in Pblec. After five washes in PBT, embryos were incubated with Cy5-labeled secondary antibody diluted 1:100 in PBS, 0.5% BSA, 0.25% Tween-20. Finally, embryos were washed three times in PBS, post-fixed for 1 min in 4% paraformaldehyde and mounted.

Mouse imaging by CT-A

Mice were anesthetized with an isoflurane/O_2 mix and tail vein cannulated for the delivery of approximately 0.1 ml of gold nanoparticles per 25 g of mouse weight. Animal temperature was maintained at 37°C and physiological monitoring was recorded. Whole body CT scans were acquired with mice placed in the supine position 4 h post injection of gold nanoparticles using a nanoScanPET/CT scanner (Mediso, Hungary) with a 50 kVP X-ray source, 300 ms exposure time in 720 projections with an acquisition time of 15 min. CT images were reconstructed in voxel size 68 x 68 x 68 μm using Nucline (Mediso, Hungary) software. Image analysis and 3D visualization was performed using VivoQuant (inviCRO version 1.23patch3) software.

Mouse imaging by Doppler ultrasound

A Vevo 2100 imaging station (VisualSonics Inc., Toronto, ON, Canada) was used for ultrasound imaging. A VisualSonics MS-550D (central frequency 40 MHz, axial resolution 40 μm, lateral resolution 90 μm, image depth 15 mm, image width 14 mm) was used for data acquisition. Mice were anesthetized with an isoflurane/O_2 mix and placed on a heated imaging stage maintained at 37°C. The body temperature, heart rate and respiratory rate were closely monitored throughout each imaging session. Abdominal hair was removed using a depilatory cream (Veet, Reckitt Benckiser, UK) and rinsed with warm water. Pre-warmed ultrasound gel (UltrasoundGel.co.uk) was then placed on the abdomen. Flow velocity waveforms of vascular lesions were obtained by locating with color Doppler, power Doppler and then placing the pulsed wave Doppler sample gate within the vessels and at the appropriate angle relative to flow direction. 2D-guided M-mode images were obtained to measure maximum vessel diameter. Image analysis was performed using the VisualSonics Vevo 2100 software package.

Retinal angiogenesis

Newborn pups (P1) were injected intragastrically with 5 μg 4-OHT (dissolved in absolute ethanol). P6 eyes were harvested and fixed 1 h in 4% PFA at 4°C and washed in PBS. Retinas were dissected, stained with IB4 and flat-mounted, or processed for immunostaining*(57)*. For immunostaining, fixed retinas were blocked and permeabilized using blocking buffer (1% BSA, 0.3% Triton X-100 in PBS) for 4 h at 4°C, then incubated overnight at 4°C with the corresponding primary antibodies in blocking buffer and washed in PBT (3 x 10 min). After 30 min incubation in Pblec, retinas were incubated for 2 h with the corresponding labelled secondary antibody and IB4 in Pblec, washed with PBT (3 x 10 min), post-fixed with 4% paraformaldehyde for 1 min and flat-mounted.

***In vivo* EC proliferation**

Pups were injected intraperitoneally with 50 µl of EdU (diluted to 2 mM in 1:1 DMSO-PBS) 2 h

before harvesting of the eyes. Detection of EdU was done using Click IT® EdU Alexa Fluor®647

(Life Technologies) according to the manufacturer's instructions. Retinas were then labelled with

the corresponding antibodies and IB4 as described above. Retinas were imaged with a Zeiss LSM

700 confocal microscope. EdU-positive nuclei were counted as proliferating ECs in a 100 μm^2

region at the angiogenic front or plexus using the ImageJ software.

RNA extraction and quantitative PCR

Total RNA was extracted from control and EC-*Pik3ca^{H1047R}* P6 mouse lungs using the RNeasy Plus

MiniKit (#74134, QIAGEN) according to the manufacturer's protocol. Samples were quality-

controlled and quantified using a Nanodrop ND-100 spectrophotometer. Reverse transcription of

total RNA was performed using a High-Capacity cDNA Reserve Transcription Kit (#4368814,

Applied BiosystemsTM). Real-time quantitative PCR was performed using TaqMan Gene

Expression Assays (Applied Biosystems) and the proprietary TaqMan Gene Expression assay

FAM/TAMRA primers (Applied Biosystems) for Pdgfb (Mm00440678_m1), Ephb4

(Mm00438750_m1), Efnb2 (Mm01215897_m1), Nr2f2 (Mm00772789_m1), and Hprt

(Mm00446968_m1). Pdgfb, Ephb4, Efnb2 and Nr2f2 mRNA expression was normalized to the

mRNA of the housekeeping gene *Hprt*.

***In vivo* rapamycin treatment**

Rapamycin was dissolved at 10 mg/ml in absolute ethanol and used as such for intraperitoneal

injection in pups at P1 and P6 at 4 mg per kg. For adult mice, the 10 mg/ml stock of rapamycin in

absolute ethanol was dissolved further in 5% polyethylene glycol (PEG-400) and 5% Tween-80 in

PBS to 0.5 mg/ml. Mice were dosed with 4 mg rapamycin per kg by intraperitoneal injection every

other day for a total of 28 days. This dose was based on previous studies using long-term rapamycin treatment *(42,43)*.

Statistics

GraphPad Prism 6 was used for all statistical analysis. Means were compared between two groups using the nonparametric Mann–Whitney U test. All statistical tests and sample size have been indicated in the figure legends.

List of Supplemental Materials

Supplemental Data include 6 figures and 3 tables.

Figure S1. Cre-mediated mosaic recombination in the *T-CreER^{T2}* mouse line.

Figure S2. Body weight over time and organ size at 6-month-old of WT and MosMes-*Pik3ca^{H1047R}* mice.

Figure S3. Whole-mount endomucin-stained E9.5 embryos dosed with 170 µg 4-OHT at E7.5.

Figure S4. MosMes-*Pik3ca^{H1047R}* mouse with a subcutaneous vascular malformation and dilated vein.

Figure S5. Genetic strategy to activate *Pik3ca^{H1047R}* in ECs.

Figure S6. Diameter of the inferior *vena cava* in a MosMes-*Pik3ca^{H1047R}* mouse before and after 28 days treatment with rapamycin.

Supplementary Table 1. List of organs and tissues subjected to histological examination (H&E staining) in WT and MosMes-*Pik3ca^{H1047R}* mice

Supplementary Table 2. Percentage of MosMes-*Pik3ca^{H1047R}* mice with VMs after dosing pregnant females with different doses of 4-OHT

Supplementary Table 3. Percentage of live WT and MosMes-*Pik3ca^{H1047R}* offspring obtained after administration of different doses of 4-OHT to pregnant females.

References and Notes:

1. B. Vanhaesebroeck, L. Stephens, P. Hawkins, PI3K signalling: the path to discovery and understanding. *Nature reviews. Molecular cell biology* **13**, 195-203 (2012).
2. Y. Samuels *et al.*, High frequency of mutations of the PIK3CA gene in human cancers. *Science* **304**, 554 (2004).
3. K. C. Kurek *et al.*, Somatic mosaic activating mutations in PIK3CA cause CLOVES syndrome. *American journal of human genetics* **90**, 1108-1115 (2012).
4. M. J. Lindhurst *et al.*, Mosaic overgrowth with fibroadipose hyperplasia is caused by somatic activating mutations in PIK3CA. *Nature genetics* **44**, 928-933 (2012).
5. J. B. Riviere *et al.*, De novo germline and postzygotic mutations in AKT3, PIK3R2 and PIK3CA cause a spectrum of related megalencephaly syndromes. *Nature genetics* **44**, 934-940 (2012).
6. J. H. Lee *et al.*, De novo somatic mutations in components of the PI3K-AKT3-mTOR pathway cause hemimegalencephaly. *Nature genetics* **44**, 941-945 (2012).
7. K. M. Keppler-Noreuil *et al.*, PIK3CA-related overgrowth spectrum (PROS): Diagnostic and testing eligibility criteria, differential diagnosis, and evaluation. *American journal of medical genetics. Part A* **167**, 287-295 (2015).
8. V. L. Luks *et al.*, Lymphatic and other vascular malformative/overgrowth disorders are caused by somatic mutations in PIK3CA. *The Journal of pediatrics* **166**, 1048-1054 e1041-1045 (2015).
9. K. M. Keppler-Noreuil *et al.*, Clinical delineation and natural history of the PIK3CA-related overgrowth spectrum. *American journal of medical genetics. Part A* **164A**, 1713-1733 (2014).
10. M. Uebelhoer, L. M. Boon, M. Vikkula, Vascular anomalies: from genetics toward models for therapeutic trials. *Cold Spring Harbor perspectives in medicine* **2** (2012).
11. C. E. Oduber, V. E. Gerdes, C. M. van der Horst, P. Bresser, Vascular malformations as underlying cause of chronic thromboembolism and pulmonary hypertension. *Journal of plastic, reconstructive & aesthetic surgery : JPRAS* **62**, 684-689; discussion 689 (2009).
12. A. Dompmartin, M. Vikkula, L. M. Boon, Venous malformation: update on aetiopathogenesis, diagnosis and management. *Phlebology / Venous Forum of the Royal Society of Medicine* **25**, 224-235 (2010).
13. N. Limaye *et al.*, Somatic mutations in angiopoietin receptor gene TEK cause solitary and multiple sporadic venous malformations. *Nature genetics* **41**, 118-124 (2009).
14. P. Castel *et al.*, Somatic PIK3CA mutations as a driver of sporadic venous malformations.
15. K. M. Kinross *et al.*, An activating Pik3ca mutation coupled with Pten loss is sufficient to initiate ovarian tumorigenesis in mice. *The Journal of clinical investigation* **122**, 553-557 (2012).
16. L. M. Hare *et al.*, Heterozygous expression of the oncogenic Pik3ca(H1047R) mutation during murine development results in fatal embryonic and extraembryonic defects. *Developmental biology* **404**, 14-26 (2015).
17. H. Yamaguchi, T. Niimi, Y. Kitagawa, K. Miki, Brachyury (T) expression in embryonal carcinoma P19 cells resembles its expression in primitive streak and tail-bud but not that in notochord. *Development, growth & differentiation* **41**, 253-264 (1999).
18. A. Kispert, B. G. Herrmann, Immunohistochemical analysis of the Brachyury protein in wild-type and mutant mouse embryos. *Developmental biology* **161**, 179-193 (1994).
19. P. Soriano, Generalized lacZ expression with the ROSA26 Cre reporter strain. *Nature genetics* **21**, 70-71 (1999).

20. S. Eifert, J. L. Villavicencio, T. C. Kao, B. M. Taute, N. M. Rich, Prevalence of deep venous anomalies in congenital vascular malformations of venous predominance. *Journal of vascular surgery* **31**, 462-471 (2000).

21. J. Soblet, N. Limaye, M. Uebelhoer, L. M. Boon, M. Vikkula, Variable Somatic TIE2 Mutations in Half of Sporadic Venous Malformations. *Molecular syndromology* **4**, 179-183 (2013).

22. M. Graupera *et al.*, Angiogenesis selectively requires the p110alpha isoform of PI3K to control endothelial cell migration. *Nature* **453**, 662-666 (2008).

23. M. Graupera, M. Potente, Regulation of angiogenesis by PI3K signaling networks. *Experimental cell research* **319**, 1348-1355 (2013).

24. A. Soler *et al.*, Inhibition of the p110alpha isoform of PI 3-kinase stimulates nonfunctional tumor angiogenesis. *J Exp Med* **210**, 1937-1945 (2013).

25. L. M. Hare *et al.*, Heterozygous expression of the oncogenic Pik3caH1047R mutation during murine development results in fatal embryonic and extraembryonic defects. *Developmental biology* (2015).

26. S. Claxton *et al.*, Efficient, inducible Cre-recombinase activation in vascular endothelium. *Genesis* **46**, 74-80 (2008).

27. K. L. Marcelo, L. C. Goldie, K. K. Hirschi, Regulation of endothelial cell differentiation and specification. *Circulation research* **112**, 1272-1287 (2013).

28. M. Vikkula *et al.*, Vascular dysmorphogenesis caused by an activating mutation in the receptor tyrosine kinase TIE2. *Cell* **87**, 1181-1190 (1996).

29. E. R. Andreeva, I. M. Pugach, D. Gordon, A. N. Orekhov, Continuous subendothelial network formed by pericyte-like cells in human vascular bed. *Tissue & cell* **30**, 127-135 (1998).

30. P. Lindahl, B. R. Johansson, P. Leveen, C. Betsholtz, Pericyte loss and microaneurysm formation in PDGF-B-deficient mice. *Science* **277**, 242-245 (1997).

31. M. Uebelhoer *et al.*, Venous malformation-causative TIE2 mutations mediate an AKT-dependent decrease in PDGFB. *Human molecular genetics* **22**, 3438-3448 (2013).

32. P. Lindblom *et al.*, Endothelial PDGF-B retention is required for proper investment of pericytes in the microvessel wall. *Genes & development* **17**, 1835-1840 (2003).

33. R. Loewe *et al.*, Stem cell marker upregulation in normal cutaneous vessels following pulsed-dye laser exposure and its abrogation by concurrent rapamycin administration: implications for treatment of port-wine stain birthmarks. *Journal of cutaneous pathology* **37 Suppl 1**, 76-82 (2010).

34. S. Kaylani, A. J. Theos, J. G. Pressey, Treatment of infantile hemangiomas with sirolimus in a patient with PHACE syndrome. *Pediatric dermatology* **30**, e194-197 (2013).

35. H. Yuksekkaya, O. Ozbek, M. Keser, H. Toy, Blue rubber bleb nevus syndrome: successful treatment with sirolimus. *Pediatrics* **129**, e1080-1084 (2012).

36. A. M. Hammill *et al.*, Sirolimus for the treatment of complicated vascular anomalies in children. *Pediatric blood & cancer* **57**, 1018-1024 (2011).

37. S. Riou *et al.*, Efficacy of rapamycin for refractory hemangioendotheliomas in Maffucci's syndrome. *Journal of clinical oncology : official journal of the American Society of Clinical Oncology* **30**, e213-215 (2012).

38. L. Marques *et al.*, Topical rapamycin combined with pulsed dye laser in the treatment of capillary vascular malformations in Sturge-Weber syndrome: phase II, randomized, double-blind, intraindividual placebo-controlled clinical trial. *Journal of the American Academy of Dermatology* **72**, 151-158 e151 (2015).

39. E. Boscolo *et al.*, Rapamycin improves TIE2-mutated venous malformation in murine model and human subjects. *The Journal of clinical investigation* **125**, 3491-3504 (2015).

40.   D. M. Sabatini, H. Erdjument-Bromage, M. Lui, P. Tempst, S. H. Snyder, RAFT1: a mammalian protein that binds to FKBP12 in a rapamycin-dependent fashion and is homologous to yeast TORs. *Cell* **78**, 35-43 (1994).

41.   M. Guba *et al.*, Rapamycin inhibits primary and metastatic tumor growth by antiangiogenesis: involvement of vascular endothelial growth factor. *Nature medicine* **8**, 128-135 (2002).

42.   C. Chen, Y. Liu, P. Zheng, mTOR regulation and therapeutic rejuvenation of aging hematopoietic stem cells. *Science signaling* **2**, ra75 (2009).

43.   Y. Fang *et al.*, Duration of rapamycin treatment has differential effects on metabolism in mice. *Cell metabolism* **17**, 456-462 (2013).

44.   Y. A. Wang *et al.*, A novel transgenic mice model for venous malformation. *Transgenic research* **18**, 193-201 (2009).

45.   B. Perry *et al.*, AKT1 overexpression in endothelial cells leads to the development of cutaneous vascular malformations in vivo. *Archives of dermatology* **143**, 504-506 (2007).

46.   K. M. Kinross *et al.*, Ubiquitous expression of the Pik3caH1047R mutation promotes hypoglycemia, hypoinsulinemia, and organomegaly. *FASEB journal : official publication of the Federation of American Societies for Experimental Biology* **29**, 1426-1434 (2015).

47.   C. J. Drake, C. D. Little, Exogenous vascular endothelial growth factor induces malformed and hyperfused vessels during embryonic neovascularization. *Proceedings of the National Academy of Sciences of the United States of America* **92**, 7657-7661 (1995).

48.   C. J. Drake, C. D. Little, VEGF and vascular fusion: implications for normal and pathological vessels. *The journal of histochemistry and cytochemistry : official journal of the Histochemistry Society* **47**, 1351-1356 (1999).

49.   M. Enge *et al.*, Endothelium-specific platelet-derived growth factor-B ablation mimics diabetic retinopathy. *The EMBO journal* **21**, 4307-4316 (2002).

50.   H. U. Wang, Z. F. Chen, D. J. Anderson, Molecular distinction and angiogenic interaction between embryonic arteries and veins revealed by ephrin-B2 and its receptor Eph-B4. *Cell* **93**, 741-753 (1998).

51.   C. C. Hong, Q. P. Peterson, J. Y. Hong, R. T. Peterson, Artery/vein specification is governed by opposing phosphatidylinositol-3 kinase and MAP kinase/ERK signaling. *Current biology : CB* **16**, 1366-1372 (2006).

52.   M. J. Yoon *et al.*, Localization of Tie2 and phospholipase D in endothelial caveolae is involved in angiopoietin-1-induced MEK/ERK phosphorylation and migration in endothelial cells. *Biochemical and biophysical research communications* **308**, 101-105 (2003).

53.   I. Kim *et al.*, Angiopoietin-1 regulates endothelial cell survival through the phosphatidylinositol 3'-Kinase/Akt signal transduction pathway. *Circulation research* **86**, 24-29 (2000).

54.   M. Natynki *et al.*, Common and specific effects of TIE2 mutations causing venous malformations. *Human molecular genetics* **24**, 6374-6389 (2015).

55.   E. Tzouanacou, S. Tweedie, V. Wilson, Identification of Jade1, a gene encoding a PHD zinc finger protein, in a gene trap mutagenesis screen for genes involved in anteroposterior axis development. *Molecular and cellular biology* **23**, 8553-8552 (2003).

56.   C. Schmidt, V. Wilson, D. Stott, R. S. Beddington, T promoter activity in the absence of functional T protein during axis formation and elongation in the mouse. *Developmental biology* **189**, 161-173 (1997).

57.   M. E. Pitulescu, I. Schmidt, R. Benedito, R. H. Adams, Inducible gene targeting in the neonatal vasculature and analysis of retinal angiogenesis in mice. *Nature protocols* **5**, 1518-1534 (2010).

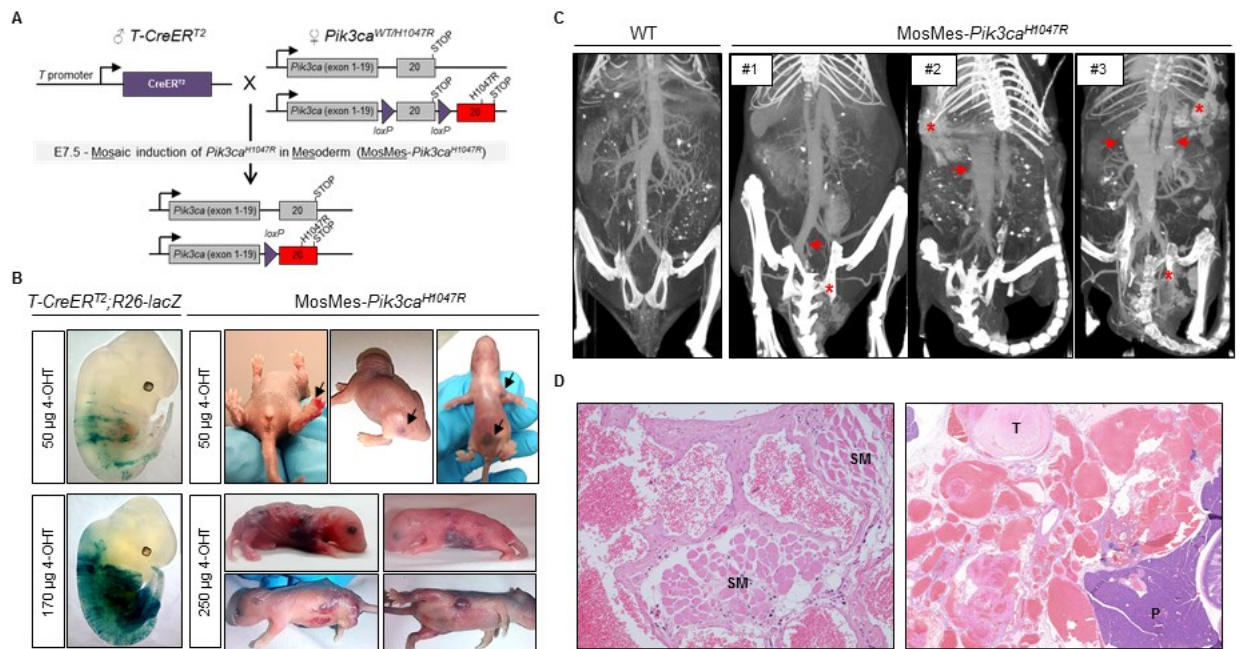**Acknowledgements**

Figures

Figure 1

Figure 1. Mosaic expression of *Pik3ca^{H1047R}* in embryonic mouse mesoderm induces vascular malformations in offspring. (**A**) Genetic strategy for mosaic *Pik3ca^{H1047R}* induction in the embryonic mesoderm. *T-CreER^{T2}* mice were crossed with *Pik3ca^{WT/H1047R}* mice that have a germline *Pik3ca* allele with a conditional H1047R mutation in exon 20. Mosaic recombination in the mesoderm is induced by a single intra-peritoneal injection of a low dose of 4-OHT to pregnant mice at E7.5. (**B**) Left, E12.5 *T-CreER^{T2};R26-lacZ* mouse embryos from pregnant mice injected with the indicated dose of 4-OHT at E7.5 and stained for β-galactosidase (β-gal) activity. Right, Representative photographs of P1-P5 MosMes-*Pik3ca^{H1047R}* pups with congenital vascular malformations (arrowed in the top panel), born to pregnant mice injected with the indicated 4-OHT dose at E7.5. (**C**) CT-A scans of adult mice four hours after intravenous injection of gold

nanoparticles. The WT mouse (left) shows normal vascular anatomy, whereas MosMes-*Pik3ca*^H1047R mice display dilatation of the left common iliac vein (arrow) and VM in the urogenital area (asterisk) (mouse #1); subcutaneous VM (asterisk) and dilatation of the inferior *vena cava* (arrow) (mouse #2); subcutaneous and urogenital VMs (asterisks) and dilatation of the inferior *vena cava* and portal vein (arrows) (mouse #3). (**D**) Representative haematoxylin and eosin (H&E)-stained sections of a subcutaneous (left) and a deep, mesenteric (right) VMs in MosMes-*Pik3ca*^H1047R mice, showing abnormal, enlarged and irregular vascular channels, most containing blood and organising fibrin thrombi (T), some with dysplastic muscular walls interposing between skeletal muscle (SM) and other tissue structures. No cytological atypia was observed. (Original magnifications x20-x200; P, pancreas).
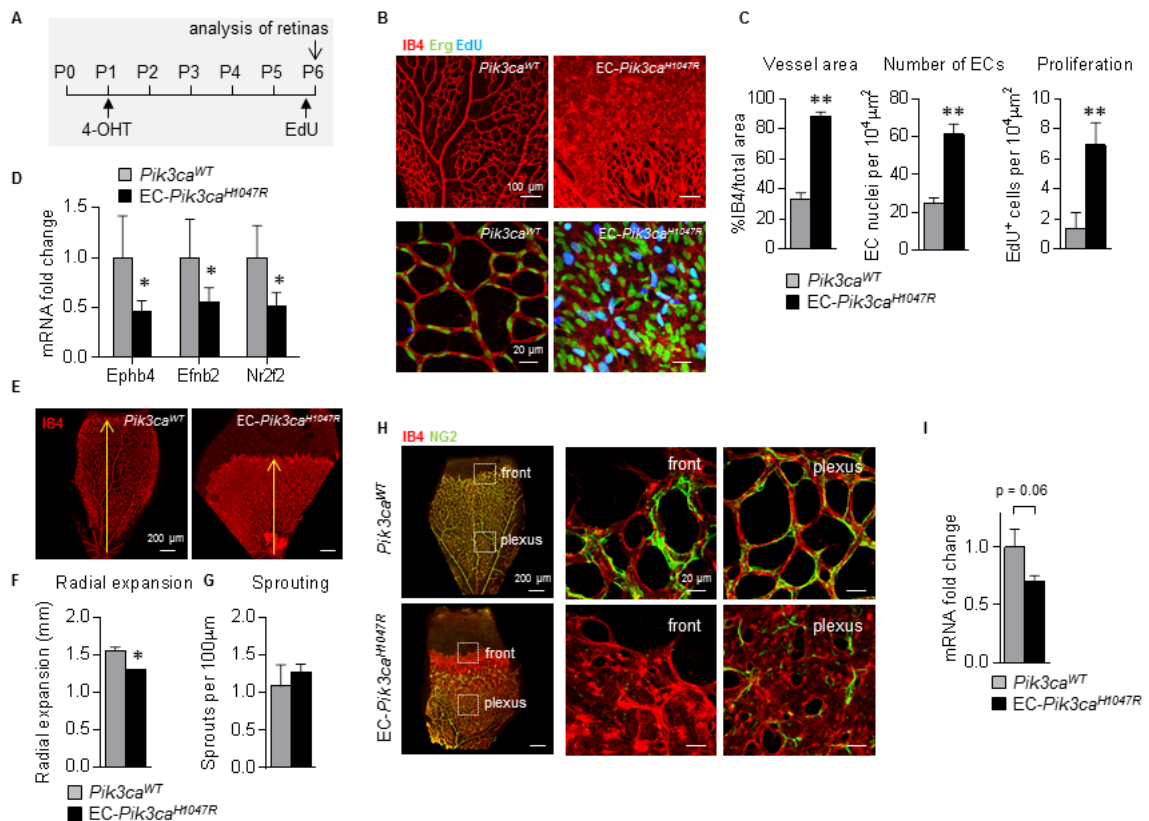
Figure 2

Figure 2. Activation of *Pik3ca^{H1047R}* in ECs promotes hyperproliferation and inhibits pericyte coverage in postnatal retinas. (**A**) Schematic of the 4-OHT and EdU administration regime used. (**B**) Representative flat-mounted *Pik3ca^{WT}* and EC-*Pik3ca^{H1047R}* P6 retinas stained with IB4 (red, revealing ECs), antibody to the Erg transcription factor (nuclear marker of ECs; green) and labelled with EdU (blue). (**C**) Quantitative analysis of the retina vessel area (assessed by IB4 staining), EC numbers (assessed by staining for Erg) and number of proliferating ECs (cells positive for both EdU and Erg). Data represent mean ± SEM. (Mann-Whitney U test) **p ≤ 0.01. n=6/genotype. (**D**) Fold change of expression of Ephb4, Efnb2, and Nr2f2 mRNA in lung lysates of *Pik3ca^{WT}* and EC-*Pik3ca^{H1047R}* P6 mice. Data represent mean ± SEM. (Mann-Whitney U test) *p < 0.05. n=5/genotype. (**E**) Representative flat-mounted control and EC-*Pik3ca^{H1047R}* P6 retinas stained with IB4. (**F**) Quantification of the radial expansion of vasculature in retinas. Data represent mean ±

SEM. (Mann-Whitney U test) *p < 0.05. n=6/genotype. (**G**) Quantification of the number of sprouts at the vascular front per unit length. Data represent mean ± SEM. n=6/genotype. (**H**) Flat-mounted *Pik3ca^{WT}* and EC-*Pik3ca^{H1047R}* retinas showing vasculature (IB4; red) and pericytes (stained for NG2, a membrane proteoglycan found in pericytes; green). **Right**, higher magnification of sections highlighted. (**I**) Fold-change of expression of Pdgfb mRNA in lung lysates of *Pik3ca^{WT}* and EC-*Pik3ca^{H1047R}* P6 mice. Data represent mean ± SEM. (Mann-Whitney U test) n=5/genotype.
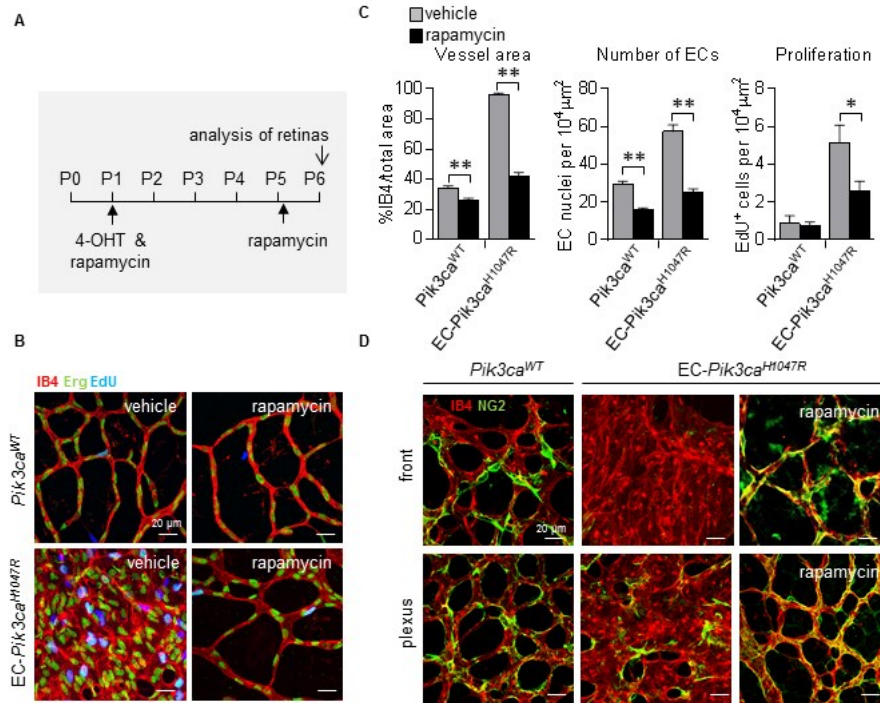
Figure 3

Figure 3. Rapamycin normalizes *Pik3ca^{H1047R}*-EC hyperproliferation and rescue pericyte coverage in postnatal retinas. (**A**) Schematic of the 4-OHT and rapamycin administration regime used for analysis of retinal angiogenesis. (**B**) Representative flat-mounted P6 retinas from vehicle and rapamycin-treated *Pik3ca^{WT}* and EC-*Pik3ca^{H1047R}* pups. Retinas are stained with IB4 (red), antibody to the Erg transcription factor (green) and labelled with EdU (blue). (**C**) Quantitative analysis of the retina vessel area (assessed by IB4 staining), EC numbers (assessed by staining for Erg) and number of proliferating ECs (cells positive for both EdU and Erg). Data represent mean ± SEM. (Mann-Whitney U test) **p ≤ 0.01, *p < 0.05. n=6/genotype. (**D**) Representative flat-mounted P6 retinas from untreated *Pik3ca^{WT}* and EC-*Pik3ca^{H1047R}* pups and rapamycin-treated EC-*Pik3ca^{H1047R}* pups showing vasculature (IB4; red) and pericytes (stained for NG2; green).
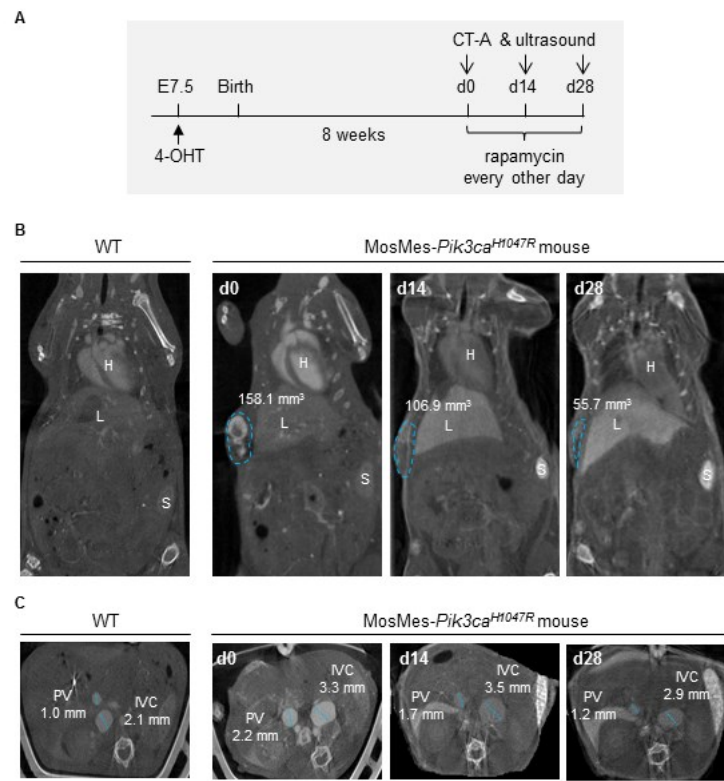
Figure 4

Figure 4. Rapamycin regress *Pik3ca^{H1047R}*-driven VMs**. (**A**) Schematic of the rapamycin therapy approach used for an adult MosMes-*Pik3ca^{H1047R}* mouse. (**B**) Measurement of the volume of the subcutaneous VM (circled in blue) from CT-A images. Indicated are the volumes of the VM. (H, heart; L, liver; S, spleen). (**C**) Measurement of the average diameter of the inferior *vena cava* and portal vein from CT-A images of an untreated WT mouse and a MosMes-*Pik3ca^{H1047R}* littermate mouse before and after 14 and 28 days of rapamycin treatment. IVC, inferior *vena cava*; PV, portal vein.

Table 1. *PIK3CA* and *TEK/*TIE2 mutations in human sporadic VMs

Patient	1	2	3	4	5	6
Age	4 years	20 years	3 years	15 years	3 years	10 years
Sex	M	M	M	M	F	F
Location of VM	Upper lip (right)	Sole of foot	Left scapular area	Right arm, chest, extensive	Face (left)	Left cheek
PIK3CA	WT	E545K (c.1633G>A)	WT	WT	WT	WT
Percent *PIK3CA* mutant allele	*NA*	6%	*NA*	*NA*	*NA*	*NA*
TEK	G1115X (c.3343G>T)	WT	Y897C (c.2690A>G), R918H (c.2753C>T)	WT	WT	WT
Percent *TEK* mutant allele	9%	*NA*	5%	*NA*	*NA*	*NA*

NA: not applicable
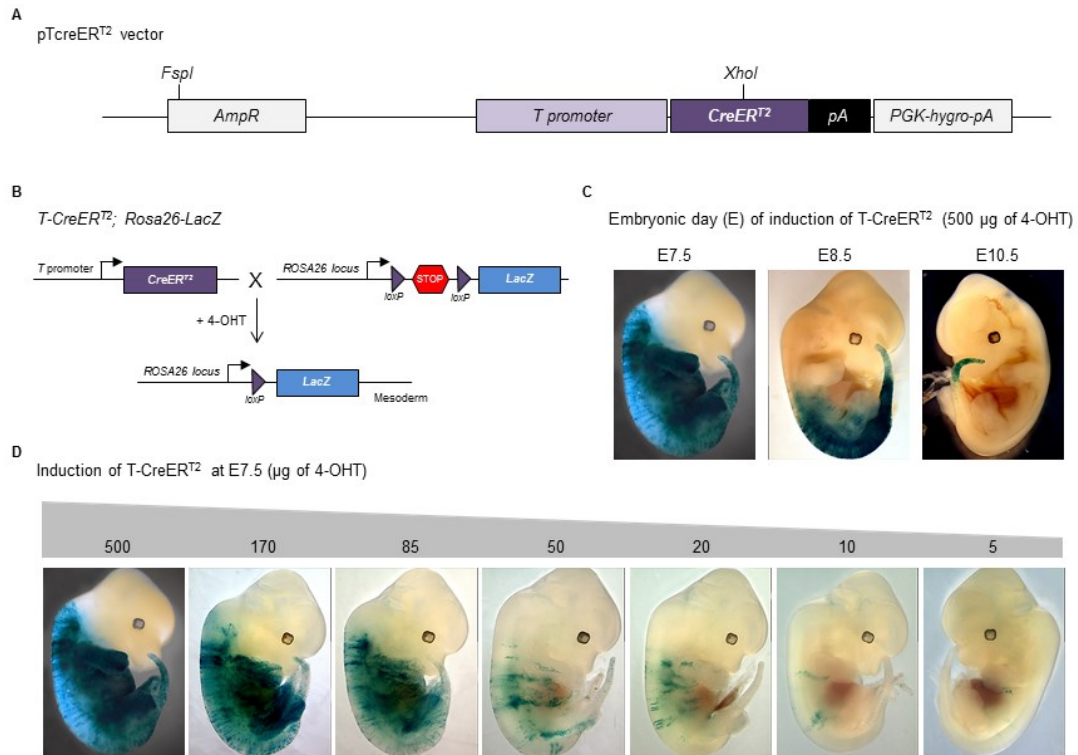
Supplementary Material

Figure S1

Figure S1. Cre-mediated mosaic recombination in the *T-CreER^{T2}* mouse line. (**A**) Schematic representation of the pTcreER^{T2} transgene used for the generation of the *T-CreER^{T2}* mouse line. (**B**) Cre-mediated recombination of the *Rosa26-lacZ* reporter inducing β-gal activity. (**C**) Whole-mount images of E12.5 *T-CreER^{T2};Rosa26-lacZ* embryos, stained for β-gal after 4-OHT administration at E7.5, E8.5 or E10.5. (**D**) same as in (C) but after 4-OHT administration at E7.5 with different doses of 4-OHT (5 to 500 μg).
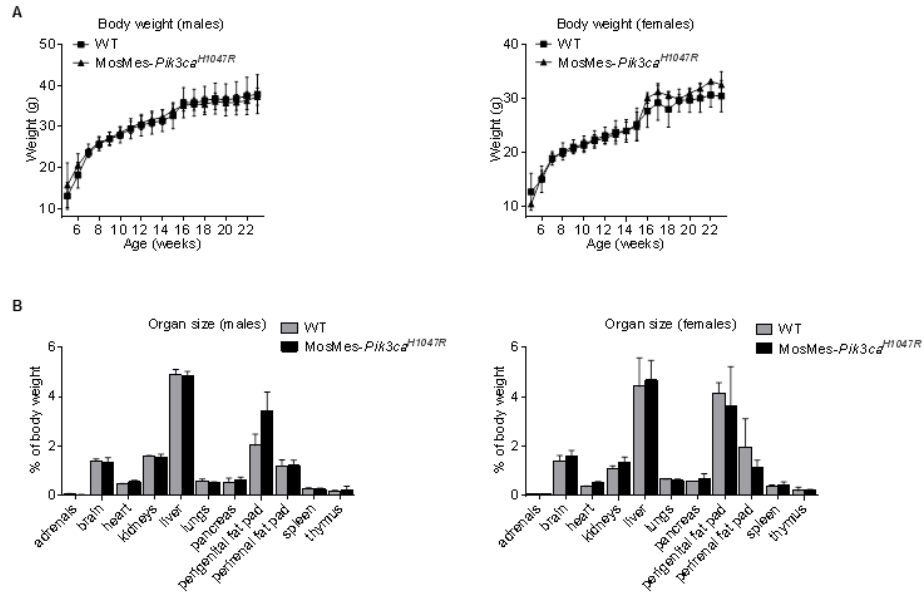
Figure S2

Figure S2. Body weight over time (**A**) and organ size at 6-month-old (**B**) of WT and MosMes-*Pik3ca^{H1047R}* mice. Data represent mean ± SEM, n=30/genotype for (A), n=6/genotype for (B).
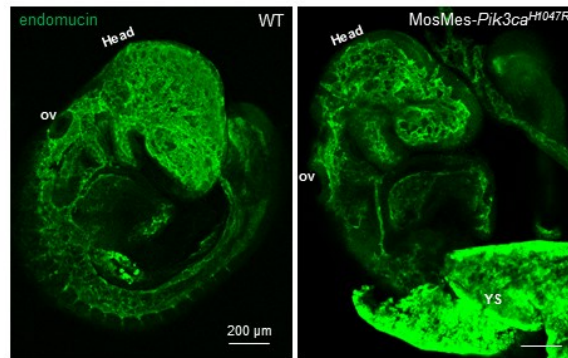
Figure S3

Figure S3. Whole-mount endomucin-stained E9.5 embryos dosed with 170 μg 4-OHT at E7.5. The MosMes-*Pik3ca*^{H1047R} embryo shows an overall less developed vasculature compared to the WT embryo. H, head; ov, otic vesicle; YS, yolk sac.
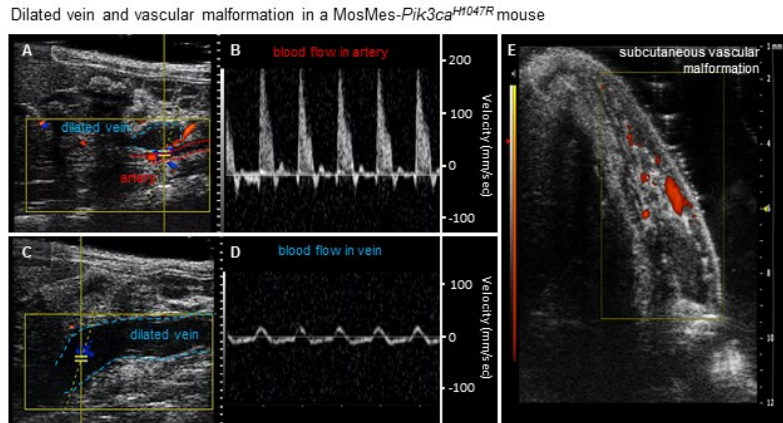
Figure S4

Dilated vein and vascular malformation in a MosMes-*Pik3ca*^{H1047R} mouse

Figure S4. MosMes-*Pik3ca*^{H1047R} mouse with a subcutaneous vascular malformation and dilated vein. (**A,C**) Ultrasound images with colour Doppler showing artery (red dotted line) and dilated vein (blue) of a Yellow markers indicate the region from which pulsed wave Doppler was acquired. (**B,D**) Pulsed wave Doppler measurement of blood flow demonstrates a high arterial flow velocity wave form within the artery (B), and a slow venous flow velocity wave form within the dilated vein (D). (**E**) Power Doppler ultrasound demonstrates slow flow signals in subcutaneous vascular malformation.
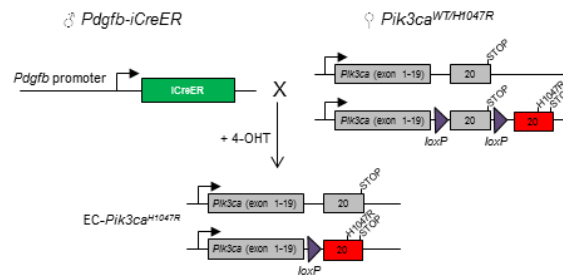
Figure S5

Figure S5. Genetic strategy to activate *Pik3ca^H1047R^* in ECs. *Pdgfb-iCreER* mice were crossed with *Pik3ca^WT/H1047R^* mice.
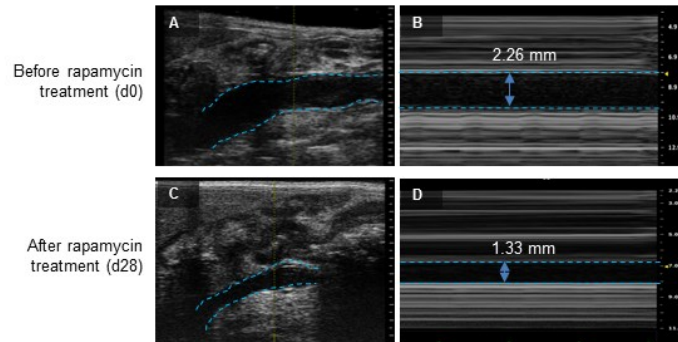
Figure S6

Figure S6. Diameter of the inferior *vena cava* in a MosMes-*Pik3ca^{H1047R}* mouse before (**A,B**) and after 28 days treatment with rapamycin (**C,D**), as revealed in 2D (**A,C**) and M mode (**B,D**) ultrasound images.

Supplementary Table 1. List of organs and tissues subjected to histological examination (H&E staining) in WT and MosMes-*Pik3ca*^{H1047R} mice

Adrenals	Ovaries/oviducts
Aorta	Pancreas
Brain	Parathyroids
Caecum	Prostate
Cervix	Rectum
Colon	Salivary gland
Duodenum	Seminal vesicles
Epididymis	Skeletal muscle
Eyes	Skin
Perigenital fat pad	Spleen
Perirenal fat pad	Sternum
Femur	Stomach
Heart	Submandibular lymph nodes
Ileum	Testes
Jejunum	Thymus
Kidneys	Thyroids
Liver	Tongue
Lungs	Trachea
Mammary glands	Urinary bladder
Oesophagus	Uterus/vagina

Supplementary Table 2. Percentage of MosMes-*Pik3ca^{H1047R}* mice with VMs after dosing pregnant females with different doses of 4-OHT

µg 4-OHT administered per pregnant mouse	MosMes-*Pik3ca^{H1047R}* mice with VMs
12.5	12.5%
50	15%
250	100%

Supplementary Table 3. Percentage of live WT and MosMes-*Pik3ca^{H1047R}* offspring obtained after administration of different doses of 4-OHT to pregnant females. The expected normal Mendelian distribution is 50% of each genotype.

	observed frequency	
µg 4-OHT administered per pregnant mouse	WT	MosMes-*Pik3ca^{H1047R}*
12.5	50.0%	50.0%
50	48.7%	51.3%
250	61.5%	38.5%